Supplementary Materials

Controllable Epitaxy of $CrTe_2$ Thin Films for Application of Saturable Absorber

Zhitao Wu‡[a], Yueqian Chen‡[b], Peiyao Xiao[a], Xu Zhang[a], Wenjun Liu*[b], Wende Xiao*[a]

Fig. S1 shows the AFM images of $CrTe_2$ films on gold-coated plane mirror at various substrate temperatures and growth times. The AFM image of clean gold-coated plane mirrors is shown in Fig. S1a. Some cracks are observed on the surface of gold coating layer. Fig. S1b-f depict $CrTe_2$ films grown at different substrate temperatures with a fixed growth time of 30 min, while Fig. S1g-h show $CrTe_2$ films grown with different growth times at a fixed substrate temperature of 285 °C. At low growth temperatures, the $CrTe_2$ films tend to form dense isolated islands with small areas and rough surfaces due to the low mobility of the deposited atoms. When the growth temperature reaches 285 °C (Fig. S1e), the $CrTe_2$ films exhibit lager domain size and flatter surface with fewer clusters. Extending the growth time yields thicker $CrTe_2$ islands with greater coverage and invisibility of the cracks. Moreover, the islands present triangular or hexagonal shapes with distinct triangular flakes on the surface (inset of Fig. S1h). This suggests that the influence of substrate on the morphology of thin films becomes weaker with increasing film thickness, resulting in regular island shapes that reflects the crystal symmetry of $CrTe_2$ at thermodynamic equilibrium states.

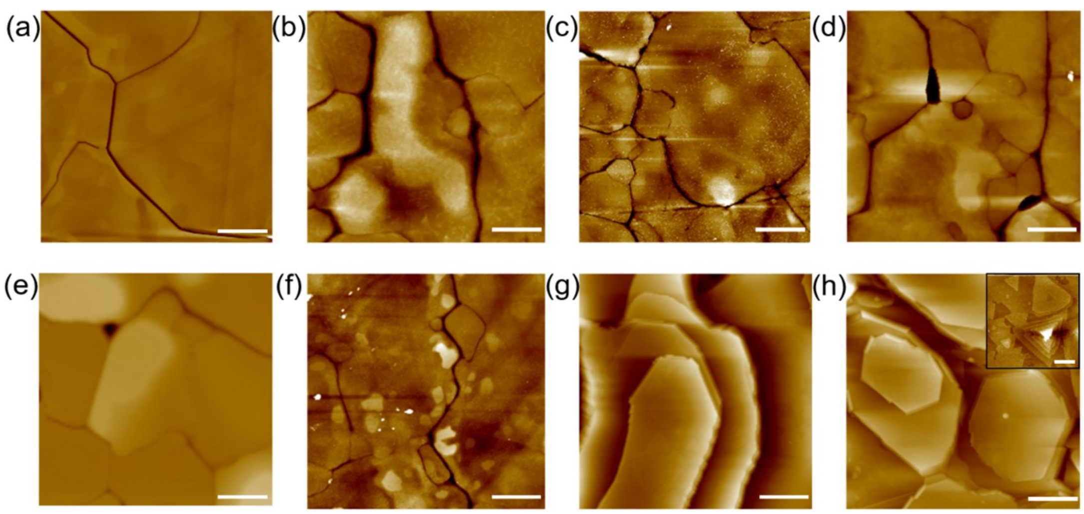

Figure S1. Evolution of the morphologies of $CrTe_2$ films grown on gold-coated plane mirrors by adjusting growth temperature and growth time. (a) AFM image of clean gold-coated plane mirrors. AFM topographies of $CrTe_2$ films grown at (b) 25 °C, (c) 120°C, (d) 200 °C, (e) 285°C, (f) 325°C. Scale bar: 2 μm. (g-h) AFM images presenting the morphological evolution of $CrTe_2$ films by adjusting the growth times of (g) 60 min and (h) 120 min at a fixed substrate temperature of 285 °C. Scale bar, 600 nm. The inset of (h) shows the distinct triangular flakes on the surface. Scale bar, 200 nm.

The dual arm balance detection optical path (Figure S2) was adopted for measuring the nonlinear energy-dependent transmission curve of the prepared $CrTe_2$-SAs.

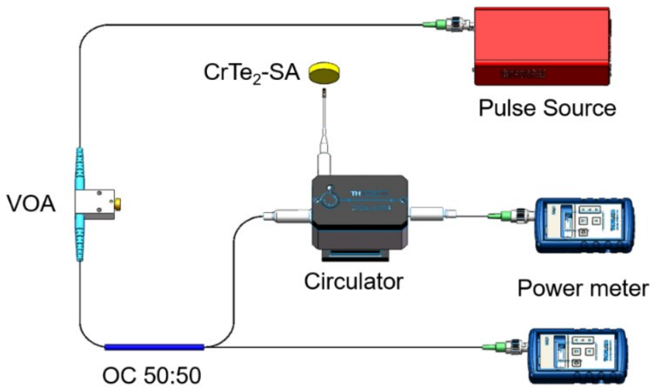

Figure S2. Dual arm balance detection optical path

At a pump power of 630 mW, we also obtained the output of Q-switched pulses in $CrTe_2$-SA based erbium-doped fiber laser (EDFL) by adjusting polarization controller (PC). Figure S.3a depicts the spectrum of Q-switching. The spectrum shows that the system is operating with a wavelength of ~ 1540 nm. When we scaled the pulse sequence of the oscilloscope to a single pulse, we found that the shortest pulse width was 660 ns, as shown in in Figure S.3b. Figure S.3c presents the RF spectrum with a measurement range of 250 kHz and a resolution bandwidth of 300 Hz, where the fundamental frequency signal of 163.9 kHz has a signal to noise ratio (SNR) of over 54.86 dB. No other frequency components in the wider span RF spectrum can be observed in Figure S.3c, except for the fundamental and doubling frequencies, which further confirms the high stability of the fiber lasers.

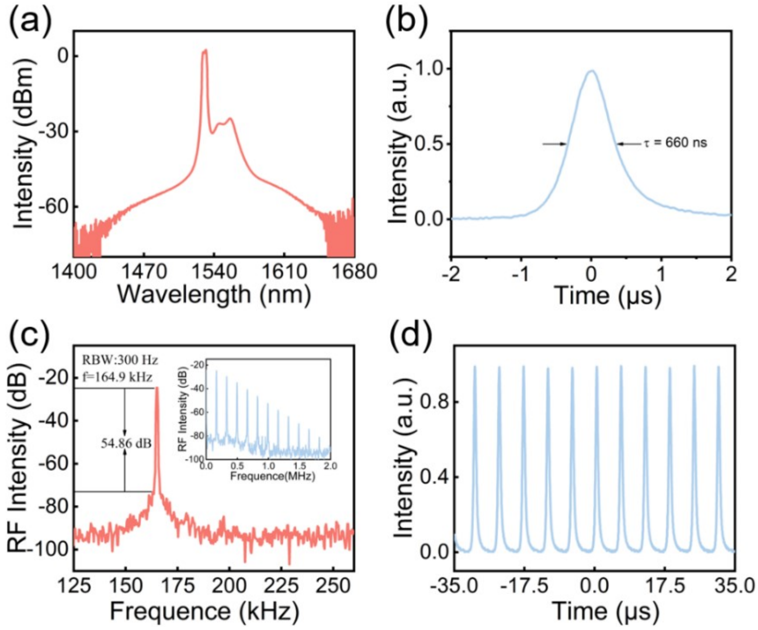

Figure S3. Output of Q-switched pulses in $CrTe_2$-SA based erbium-doped fiber laser (EDFL). (a) the spectrum of Q-switching based on the $CrTe_2$-SA. (b) the single pulse sequence based on the $CrTe_2$-SA. (c) the RF spectrum based on the $CrTe_2$-SA. (d) Pulse train based on the $CrTe_2$-SA.